The Astronomical Journal, 163:207 (26pp), 2022 May https://doi.org/10.3847/1538-3881/ac517f

A Possible Alignment Between the Orbits of Planetary Systems and their Visual Binary Companions

Sam Christian[1,2], Andrew Vanderburg[1,3], Juliette Becker[4,90], Daniel A. Yahalomi[5], Logan Pearce[6,91], George Zhou[7,8], Karen A. Collins[7], Adam L. Kraus[9], Keivan G. Stassun[10,11], Zoe de Beurs[1,9], George R. Ricker[1], Roland K. Vanderspek[1], David W. Latham[7], Joshua N. Winn[12], S. Seager[1,13,14], Jon M. Jenkins[15], Lyu Abe[16], Karim Agabi[16], Pedro J. Amado[17], David Baker[18], Khalid Barkaoui[19,20], Zouhair Benkhaldoun[20], Paul Benni[21], John Berberian[22], Perry Berlind[7], Allyson Bieryla[7], Emma Esparza-Borges[23,24], Michael Bowen[25,26], Peyton Brown[27], Lars A. Buchhave[28], Christopher J. Burke[1], Marco Buttu[29], Charles Cadieux[30], Douglas A. Caldwell[31], David Charbonneau[7], Nikita Chazov[32], Sudhish Chimaladinne[25], Kevin I. Collins[25], Deven Combs[25,33], Dennis M. Conti[34], Nicolas Crouzet[35], Jerome P. de Leon[36], Shila Deljookorani[37], Brendan Diamond[37], René Doyon[30,38], Diana Dragomir[39], Georgina Dransfield[40], Zahra Essack[13,41], Phil Evans[42], Akihiko Fukui[24,43], Tianjun Gan[44], Gilbert A. Esquerdo[7], Michaël Gillon[45], Eric Girardin[46], Pere Guerra[47], Tristan Guillot[16], Eleanor Kate K. Habich[48], Andreea Henriksen[28], Nora Hoch[48], Keisuke I Isogai[49,50], Emmanuël Jehin[51], Eric L. N. Jensen[52], Marshall C. Johnson[53], John H. Livingston[36], John F. Kielkopf[54], Kingsley Kim[25,33], Kiyoe Kawauchi[50], Vadim Krushinsky[32], Veronica Kunzle[37], Didier Laloum[55], Dominic Leger[37], Pablo Lewin[56], Franco Mallia[57], Bob Massey[58], Mayuko Mori[36], Kim K. McLeod[48], Djamel Mékarnia[16], Ismael Mireles[59], Nikolay Mishevskiy[60], Motohide Tamura[61,62,63], Felipe Murgas[64,65], Norio Narita[43,62,66,67,68], Ramon Naves[69], Peter Nelson[70], Hugh P. Osborn[1,71], Enric Palle[70,73], Hannu Parviainen[72,73], Peter Plavchan[25], Francisco J. Pozuelos[45,74], Markus Rabus[75], Howard M. Relles[7], Cristina Rodríguez López[17], Samuel N. Quinn[7], Francois-Xavier Schmider[16], Joshua E. Schlieder[76], Richard P. Schwarz[77], Avi Shporer[1], Laurie Sibbald[78,92], Gregor Srdoc[79], Caitlin Stibbards[25], Hannah Stickler[48], Olga Suarez[16], Chris Stockdale[80], Thiam-Guan Tan[81,82], Yuka Terada[83,84], Amaury Triaud[40], Rene Tronsgaard[28], William C. Waalkes[85], Gavin Wang[86,87], Noriharu Watanabe[50], Marie-Sainte Wenceslas[29], Geof Wingham[88], Justin Wittrock[25], and Carl Ziegler[89]

[1] Department of Physics and Kavli Institute for Astrophysics and Space Research, Massachusetts Institute of Technology, Cambridge, MA 02139, USA; samchristian@mit.edu
[2] Liberal Arts and Science Academy, Austin, TX 78724, USA
[3] Department of Astronomy, University of Wisconsin-Madison, Madison, WI 53706, USA
[4] Division of Geological and Planetary Sciences, California Institute of Technology, Pasadena, CA 91125, USA
[5] Department of Astronomy, Columbia University, 550 W 120th Street, New York, NY 10027, USA
[6] Steward Observatory, University of Arizona, Tucson, AZ 85721, USA
[7] Center for Astrophysics | Harvard & Smithsonian, 60 Garden Street, Cambridge, MA 02138, USA
[8] Centre for Astrophysics, University of Southern Queensland, Toowoomba, Queensland 4350, Australia
[9] Department of Astronomy, University of Texas at Austin, Austin, TX 78712, USA
[10] Department of Physics and Astronomy, Vanderbilt University, 6301 Stevenson Center Lane, Nashville, TN 37235, USA
[11] Department of Physics, Fisk University, 1000 17th Avenue North, Nashville, TN 37208, USA
[12] Department of Astrophysical Sciences, Princeton University, 4 Ivy Lane, Princeton, NJ 08544, USA
[13] Department of Earth, Atmospheric and Planetary Sciences, Massachusetts Institute of Technology, Cambridge, MA 02139, USA
[14] Department of Aeronautics and Astronautics, MIT, 77 Massachusetts Avenue, Cambridge, MA 02139, USA
[15] NASA Ames Research Center, Moffett Field, CA 94035, USA
[16] Université Côte d'Azur, Observatoire de la Côte d'Azur, CNRS, Laboratoire Lagrange, Bd de l'Observatoire, CS 34229, F-06304 Nice cedex 4, France
[17] Instituto de Astrofísica de Andalucía (IAA-CSIC), Glorieta de la Astronomía s/n, E-18008 Granada, Spain
[18] Physics Department, Austin College, Sherman, TX 75090, USA
[19] Astrobiology Research Unit, Université de Liège, 19C Allée du 6 Août, B-4000 Liège, Belgium
[20] Oukaimeden Observatory, High Energy Physics and Astrophysics Laboratory, Cadi Ayyad University, Marrakech, Morocco
[21] Acton Sky Portal (Private Observatory), Acton, MA, USA
[22] Woodson High School, 9525 Main St, Fairfax, VA 22031, USA
[23] Departamento de Astrofísica, Universidad de La Laguna (ULL), E-38206 La Laguna, Tenerife, Spain
[24] Instituto de Astrofísica de Canarias, Vía Láctea s/n, E-38205 La Laguna, Tenerife, Spain
[25] George Mason University, 4400 University Drive, Fairfax, VA 22030 USA
[26] Millennium Institute for Astrophysics, Chile
[27] Vanderbilt University, 2201 West End Avenue, Nashville, TN 37235, USA
[28] DTU Space, National Space Institute, Technical University of Denmark, Elektrovej 328, DK-2800 Kgs. Lyngby, Denmark
[29] PNRA, IPEV, Concordia Station, Antarctica
[30] Université de Montréal, Département de Physique, IREX, Montréal, QC H3C 3J7, Canada
[31] SETI Institute, Mountain View, CA 94043, USA
[32] Kourovka Observatory, Ural Federal University, 19 Mira street, Yekaterinburg, Russia
[33] Thomas Jefferson High School, for Science and Technology, 6560 Braddock Rd, Alexandria, VA 22312, USA
[34] American Association of Variable Star Observers, 49 Bay State Road, Cambridge, MA 02138, USA
[35] European Space Agency (ESA), European Space Research and Technology Centre (ESTEC), Keplerlaan 1, 2201 AZ Noordwijk, The Netherlands
[36] Department of Astronomy, Graduate School of Science, The University of Tokyo, 7-3-1 Hongo, Bunkyo-ku, Tokyo 113-0033, Japan
[37] Howard Community College, 10901 Little Patuxent Pkwy, Columbia, MD 21044, USA
[38] Observatoire du Mont-Mégantic, Université de Montréal, Montréal, QC H3C 3J7, Canada
[39] Department of Physics and Astronomy, University of New Mexico, 1919 Lomas Boulevard NE, Albuquerque, NM 87131, USA
[40] School of Physics & Astronomy, University of Birmingham, Edgbaston, Birmingham, B15 2TT, UK
[41] Kavli Institute for Astrophysics and Space Research, Massachusetts Institute of Technology, Cambridge, MA 02139, USA
[42] El Sauce Observatory, Coquimbo Province, Chile
[43] Komaba Institute for Science, The University of Tokyo, 3-8-1 Komaba, Meguro, Tokyo 153-8902, Japan

[44] Department of Astronomy and Tsinghua Centre for Astrophysics, Tsinghua University, Beijing 100084, People's Republic of China
[45] Astrobiology Research Unit, Université de Liège, 19C Allèe du 6 Août, B-4000 Liège, Belgium
[46] Grand Pra Observatory, Switzerland
[47] Observatori Astronòmic Albanyà, Camí de Bassegoda S/N, Albanyà E-17733, Girona, Spain
[48] Department of Astronomy, Wellesley College, Wellesley, MA 02481, USA
[49] Okayama Observatory, Kyoto University, 3037-5 Honjo, Kamogatacho, Asakuchi, Okayama 719-0232, Japan
[50] Department of Multi-Disciplinary Sciences, Graduate School of Arts and Sciences, The University of Tokyo, 3-8-1 Komaba, Meguro, Tokyo 153-8902, Japan
[51] Space Sciences, Technologies and Astrophysics Research (STAR), Institute, Université de Liège, 19C Allée du 6 Août, B-4000 Liège, Belgium
[52] Dept. of Physics & Astronomy, Swarthmore College, Swarthmore, PA 19081, USA
[53] Department of Astronomy, Ohio State University, 140 West 18th Avenue, Columbus, OH 43210, USA
[54] Department of Physics and Astronomy, University of Louisville, Louisville, KY 40292, USA
[55] Société Astronomique de France, 3 Rue Beethoven, F-75016 Paris, France
[56] The Maury Lewin Astronomical Observatory, Glendora, CA 91741, USA
[57] Campo Catino Astronomical Observatory, Regione Lazio, Guarcino (FR), I-03010, Italy
[58] Villa '39 Observatory, Landers, CA 92285, USA
[59] Department of Physics and Astronomy, University of New Mexico, 210 Yale Boulevard NE, Albuquerque, NM 87106, USA
[60] Private Astronomical Observatory, Nezavisimosti 114g, Ananjev, Odessa region, 66400, Ukraine
[61] Department of Astronomy, University of Tokyo, 7-3-1 Hongo, Bunkyo-ku, Tokyo 113-0033, Japan
[62] Astrobiology Center, 2-21-1 Osawa, Mitaka-shi, Tokyo 181-8588, Japan
[63] National Astronomical Observatory, 2-21-1 Osawa, Mitaka-shi, Tokyo 181-8588, Japan
[64] Instituto de Astrofísica de Canarias (IAC), E-38205 La Laguna, Tenerife, Spain
[65] Departamento de Astrofísica, Universidad de La Laguna (ULL), E-38206 La Laguna, Tenerife, Spain
[66] JST, PRESTO, 3-8-1 Komaba, Meguro, Tokyo 153-8902, Japan
[67] National Astronomical Observatory of Japan, 2-21-1 Osawa, Mitaka, Tokyo 181-8588, Japan
[68] Instituto de Astrofisica de Canarias (IAC), 38205 La Laguna, Tenerife, Spain
[69] Observatory Montcabrerm MPC 213 Cabrils, Barcelona, Spain
[70] AAVSO, 5 Inverness Way, Hillsborough, CA 94010, USA
[71] NCCR/PlanetS, Centre for Space & Habitability, University of Bern, Bern, Switzerland
[72] Instituto de Astrofísica de Canarias (IAC), E-38205 La Laguna, Tenerife, Spain
[73] Departamento de Astrofísica, Universidad de La Laguna (ULL), E-38206, La Laguna, Tenerife, Spain
[74] Space Sciences, Technologies and Astrophysics Research (STAR) Institute, Université de Liège, 19C Allèe du 6 Août, B-4000 Liège, Belgium
[75] Departamento de Matemática y Física Aplicadas, Facultad de Ingeniería, Universidad Católica de la Santísima Concepción, Alonso de Rivera 2850, Concepción, Chile
[76] NASA Goddard Space Flight Center, 8800 Greenbelt Rd, Greenbelt, MD 20771, USA
[77] Patashnick Voorheesville Observatory, Voorheesville, NY 12186, USA
[78] RASC Calgary Alberta, Calgary, AB T2P 4J3, Canada
[79] Kotizarovci Observatory, Sarsoni 90, 51216 Viskovo, Croatia
[80] Hazelwood Observatory, Australia
[81] Perth Exoplanet Survey Telescope, Perth, Australia
[82] Curtin Institute of Radio Astronomy, Curtin University, Bentley, 6102, Australia
[83] Institute of Astronomy and Astrophysics, Academia Sinica, P.O. Box 23-141, Taipei 10617, Taiwan, R.O.C.
[84] Department of Astrophysics, National Taiwan University, Taipei 10617, Taiwan, R.O.C.
[85] Department of Astrophysical and Planetary Sciences, University of Colorado, Boulder, CO 80309, USA
[86] Tsinghua International School, Beijing 100084, People's Republic of China
[87] Stanford Online High School, 415 Broadway Academy Hall, Floor 2, 8853, Redwood City, CA 94063, USA
[88] Mt. Stuart Observatory, New Zealand
[89] Department of Physics, Engineering and Astronomy, Stephen F. Austin State University, 1936 North Street, Nacogdoches, TX 75962, USA
Received 2021 June 22; revised 2021 December 21; accepted 2022 January 30; published 2022 April 11

Abstract

Astronomers do not have a complete picture of the effects of wide-binary companions (semimajor axes greater than 100 au) on the formation and evolution of exoplanets. We investigate these effects using new data from Gaia Early Data Release 3 and the Transiting Exoplanet Survey Satellite mission to characterize wide-binary systems with transiting exoplanets. We identify a sample of 67 systems of transiting exoplanet candidates (with well-determined, edge-on orbital inclinations) that reside in wide visual binary systems. We derive limits on orbital parameters for the wide-binary systems and measure the minimum difference in orbital inclination between the binary and planet orbits. We determine that there is statistically significant difference in the inclination distribution of wide-binary systems with transiting planets compared to a control sample, with the probability that the two distributions are the same being 0.0037. This implies that there is an overabundance of planets in binary systems whose orbits are aligned with those of the binary. The overabundance of aligned systems appears to primarily have semimajor axes less than 700 au. We investigate some effects that could cause the alignment and conclude that a torque caused by a misaligned binary companion on the protoplanetary disk is the most promising explanation.

[90] 51 Pegasi b Fellow.
[91] NSF Graduate Research Fellow.
[92] Citizen Scientist.

Unified Astronomy Thesaurus concepts: Star-planet interactions (2177); Circumstellar disks (235); Exoplanet evolution (491); Wide binary stars (1801); Visual binary stars (1777)

Supporting material: machine-readable tables

1. Introduction

Many stars in our galaxy reside in binary systems (Fischer & Marcy 1992; Frankowski et al. 2007; Raghavan et al. 2010). These binary systems have semimajor axes ranging from less than 0.01 au (Dimitrov & Kjurkchieva 2010) to greater than 20,000 au (Latham et al. 1991; Jiménez-Esteban et al. 2019). The extreme range in semimajor axes exhibited by binary systems makes it very challenging for any one formation mechanism to explain all observed systems; instead, there are likely multiple pathways by which binary stars may form.

At close separations, binary stars with semimajor axes less than about 100 au may form by disk fragmentation (Adams et al. 1989) and turbulent fragmentation at larger separations followed by migration (Bate 2018). In disk fragmentation, instabilities in massive circumstellar disks collapse and form a second star orbiting in the plane of the disk. At larger separations, binary stars can form through turbulent fragmentation, where turbulence in the initial core leads to fragmentation of the core into an eventual wide-binary system (Offner et al. 2010, 2016; Bate 2018). These binaries can in turn migrate to smaller separations; thus, close binaries form through a mixture of disk and turbulent fragmentation. Another viable mechanism for the formation of wide binaries is core capture, in which initially unbounded stars form, for example, via the dissolution of open clusters (Kouwenhoven et al. 2010) or from pre-stellar core capture (Tokovinin 2017).

Many binary stars are known to host exoplanets (Mugrauer 2019). While some exoplanets orbit around *both* stars in the binary (the so-called circumbinary system; e.g., Doyle et al. 2011), most exoplanets in binary systems orbit closely around just one of the binary components (a circumstellar orbit). In wide-binary systems, it is believed that virtually all planets will be on circumstellar orbits. The effects of a wide-binary companion on a planetary system are debated. Theoretical work has shown that the dynamical influence of wide-binary companions can eject planets and increase the eccentricity of planetary orbits (Kaib et al. 2013; Correa-Otto & Gil-Hutton 2017; Bazsó & Pilat-Lohinger 2020). Binary companions can affect planetary orbits via the Lidov–Kozai mechanism (von Zeipel 1910; Kozai 1962; Lidov 1962), potentially causing tidal migration of planets to tighter orbits. This mechanism could provide an explanation for the existence of hot Jupiters (Wu & Murray 2003; Fabrycky & Tremaine 2007; Petrovich 2015; Dawson & Johnson 2018; Li et al. 2020), although this is not the only mechanism that can explain hot Jupiter orbits (Lin et al. 1996; Batygin et al. 2016; Ngo et al. 2016), and at least some hot Jupiters could not have formed in this way (e.g., Becker et al. 2015, 2017; Weiss et al. 2017; Cañas et al. 2019; Huang et al. 2020). The presence of a torque from the binary companion could also misalign the protostellar disk (Batygin 2012; Lai 2014; Hjorth et al. 2021).

On the observational front, statistical analyses have shown that while wide-binary companions with semimajor axes $\gtrsim$1000 au do not seem to have a significant impact on planet occurrence (Deacon et al. 2016), closer binary companions (of semimajor axes $\lesssim$100 au) seem to suppress planet occurrence (Kraus et al. 2016; Ziegler et al. 2021), possibly by disrupting the protoplanetary disk (Duchêne 2010).

So far, most observational studies of binary companions to exoplanet hosts have focused on the effects of binary companions as a function of the projected separation, partly due to the difficulty of determining the true separation or orbital elements of binary systems. Traditionally, measuring visual binary-star orbits requires repeated precise observations of the positions of the two stars over years, decades, or even centuries (Mason et al. 2001). However, recently the extremely precise astrometry from ESA's Gaia mission (Gaia Collaboration et al. 2016) has made it possible to derive loose constraints on the orbital elements of visual binary stars using only the masses and instantaneous relative velocities of the two components (Newton et al. 2019; Pearce et al. 2020).

Meanwhile, the advent of exoplanet-detecting space telescopes—specifically, the Kepler mission (Koch et al. 2010) and the Transiting Exoplanet Survey Satellite (TESS; Ricker et al. 2015) that use the transit method to detect exoplanets—have resulted in an explosion in the numbers of planets known in visual binaries. Because the planets discovered by Kepler and TESS transit their host stars, we know that the planetary orbital planes are aligned to within a few degrees of our line of sight.

In this paper, we take advantage of these new observations to study whether there is a tendency toward alignment in the orientation of the orbits of visual binary systems and the orbits of planets that reside in these systems. In particular, we measure the orbital inclination of a sample of visual binary stars in which one component is known to host a transiting exoplanet candidate.

It is important to note that we refer to alignment as the minimum alignment between the binary system orbit and exoplanet orbit, not the stellar rotation axis of the primary star and orbit of the exoplanet as is commonly measured using the Rossiter–McLaughlin effect. We make no assumptions on the orientation of the stellar rotation axis in our analysis.

Because the orbital inclinations of the transiting planets must be close to 90°, an overabundance of edge-on binary orbits implies a preferential alignment between the binary systems and their planets. The observed misalignment is really the minimum possible misalignment of the binary system. If Ω_p, Ω_b, i_p, and i_b are the longitude of the ascending node and the inclination of the planet and binary, respectively, then the misalignment, Δ, between the binary and planet can be expressed as

$$\cos(\Delta) = \cos(i_p)\cos(i_b) + \sin(i_p)\sin(i_b)\cos(\Omega_p - \Omega_b). \quad (1)$$

Since $i_p = 90°$,

$$\cos(\Delta) = \cos(90 - i_b)\cos(\Omega_p - \Omega_b). \quad (2)$$

Thus the observed misalignment $|90 - i_b|$ is only equivalent to the actual misalignment Δ if the longitude of the ascending nodes of the binary system and planet happen to be the same; otherwise, Δ is equivalent to the minimum misalignment between the binary system and planet. A large observed relative inclination means a system is misaligned, while a system with small observed relative inclination could be aligned or misaligned depending on the relative (unknown) longitude of the ascending nodes of the

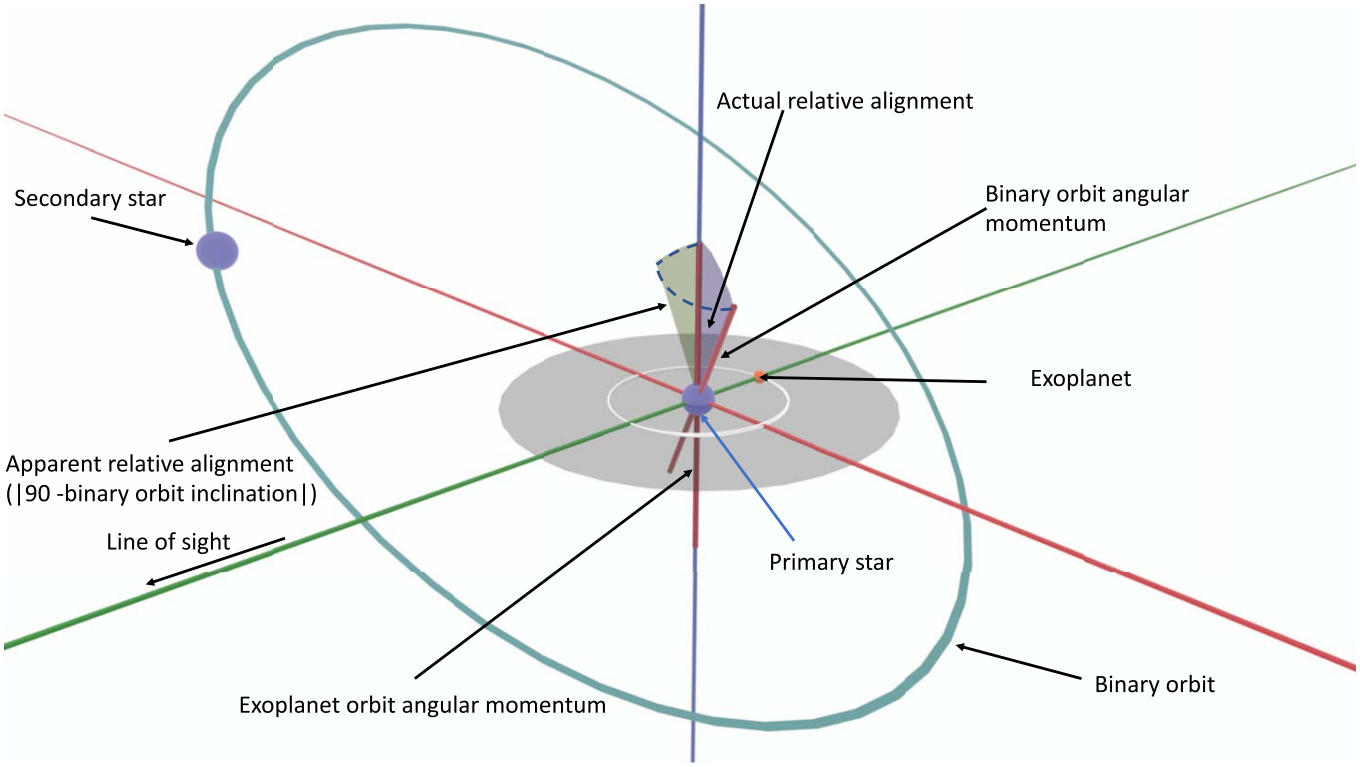

Figure 1. A diagram of the orbital configurations relevant to this paper. The diagram is centered on the primary star. Apparent relative alignment is calculated as $|90° - i|$, where i is the inclination of the binary system (the transiting exoplanets will always have approximately 90° inclination). In the diagram, the green wedge is the inclination of the binary system. The primary star is the star that hosts the exoplanet, while the binary companion is the companion star without detected exoplanets. The angular momentum of the star is the axis that the star rotates on. The exoplanet (orange) orbits at 90° to the line of sight.

exoplanet and binary orbit. However, if many systems are observed, an overabundance of small relative inclinations has the physical interpretation that an overabundance of systems tends to be aligned since the longitude of the ascending nodes of misaligned systems is expected to be distributed randomly and independently of relative inclination. A diagram of the relevant parameters described in this paper is presented in Figure 1.

This paper is organized as follows. In Section 2 we present the Gaia Early Data Release 3 (EDR3), TESS, and ground-based spectroscopic and photometric observations used in our study. In Section 3 we describe the procedure we use to constrain the masses of the binary systems and subsequently model the orbits of the binary systems. In Section 4, we describe the statistical tests performed on the data and rule out possible biases. Section 5 gives an analysis of two theoretical mechanisms that could possibly cause the observed alignment. In Section 6 we discuss two possible scenarios for the observed alignment and discuss future directions for our work. Finally, in Section 7 we summarize our results.

2. Observations/Data

To investigate whether there is a tendency toward alignment between the orbits of visual binary stars and their planetary systems, we need both a sample of likely transiting planet candidates and a constraint on the orbital inclinations of any visual binary companions to these planet host stars. For the former, we make use of planet candidates discovered by the TESS mission and vetted with ground-based follow-up photometric and spectroscopic observations. For the latter, we use astrometric observations from Gaia, archival broadband photometry, and metallicity measurements from both new and archival spectra to determine the masses of the binary components using isochrone fitting. We also perform a variety of cuts on our sample of visual binaries with exoplanets and a control sample. A diagram of the various cuts performed is shown in Figure 2. We describe these inputs to our analysis and the cuts we performed in more detail in this section.

2.1. TESS Planet Candidates

2.1.1. Identification with TESS

We start with the list of planet candidates reported by the TESS mission (also known as TESS Objects of Interest, or TOIs). TESS uses four 10 cm cameras to repeatedly image 96° by 24° regions of the sky for 28 days at a time. After the completion of each 28 day observation (called a sector), TESS moves to a new field of view and repeats the process. Over the course of its 2 year primary mission, TESS observed approximately 70% of the sky, and is continuing to observe in an extended mission.

The TESS CCDs read out images of the sky every 2 s, but the data volume required to download each 2 s image from orbit would be prohibitively large. Instead, TESS coadds the 2 s images into longer observations before beaming the data back to Earth. Most of the sky is coadded to long-cadence Full Frame Images (FFIs) with exposure times of 30 minutes (in the primary mission) or 10 minutes (in the extended mission), while the pixels surrounding 20,000 preselected stars are coadded to 2 minutes; for the extended mission, 1000 of these targets are coadded to 20 s.

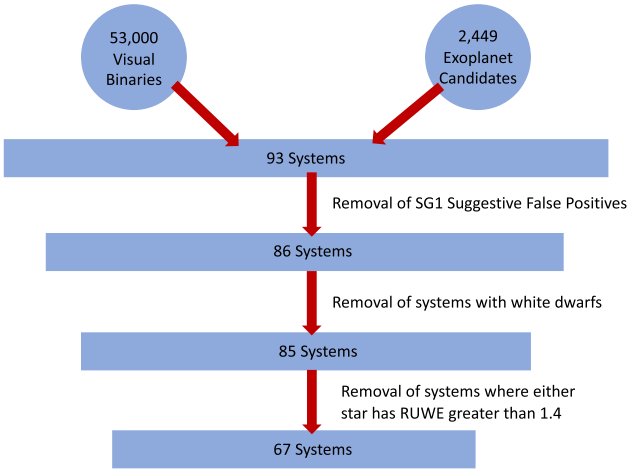

Figure 2. A hierarchy of the cuts performed on the sample of visual binaries with transiting exoplanet candidates. The same cuts were performed on the control sample. The specific cuts performed are described in detail in Section 2.

Once the data have been received on Earth, they are analyzed as described by Guerrero et al. (2021) to process the observations and identify planet candidates. We base our sample on the list of all TESS planet candidates that had been reported online as of 2020 December 15.

2.1.2. Sample of Visual Binaries with Planet Candidates

We identify planet-candidate-hosting stars that also happen to reside in a visual binary system matching the underlying Gaia DR2 ID of items in the TESS Input Catalog (TIC) to a catalog of visual binary stars identified in Gaia data by El-Badry & Rix (2018). This work reports approximately 53,000 visual binary systems within 200 pc of the Sun and with projected separations between 50 and 50,000 au derived from Gaia DR2 astrometric observations. Although the catalog has binaries with separations as small as 50 au, the vast majority of binaries in the catalog have much wider separations. At wider separations, it is more likely that the Gaia spacecraft will resolve the individual stars in the binary system. In total, after all cuts were performed, we identified a sample of 67 visual binary systems including a TESS planet-candidate host star with projected semimajor axes ranging from 61 to 34,700 au and parallaxes ranging from 5 to 48 mas.

2.1.3. Follow-up Ground-based Time-series Photometry

We identified and removed additional false-positive planet candidates using ground-based observations. The majority of these observations came from Sub-Group 1 (SG1) of the TESS Follow-up Observing Program Working Group (TFOP WG), which performs seeing-limited time-series photometry of TOIs. The specific facilities used for follow-up observations are listed in Table 1. SG1 observations have the primary purposes of ruling out the possibility of nearby eclipsing binaries (NEBs) as the source of the TESS detection and refining the parameters of transiting planet candidates.

SG1 observations are used to classify TOIs into a variety of photometric dispositions, indicating whether a given candidate is a false positive, a plausible candidate, or a well-vetted likely planet. The dispositions used by SG1 are as follows:

1. PC, or Planet Candidate, indicates that either no follow-up observations have been conducted, or that they are in progress.
2. PPC, or Promising Planet Candidate, indicates that follow-up observations have ruled out NEB false-positive scenarios on most stars in the field.
3. CPC, or Cleared Planet Candidate, indicates that follow-up observations have ruled out NEB false-positive scenarios on all stars in the field.
4. VPC, or Validated Planet Candidate, indicates that ground-based follow-up observations have detected the transit signal discovered by TESS, confirming that the signal is on-target and not a false alarm.
5. KP, or Known Planet, indicates the candidate was previously identified and confirmed as a planet independently of TESS.
6. LEPC, or Lost Ephemeris Planet Candidate, indicates that the uncertainty on predicted future transit times has grown large enough that ground-based photometric observations cannot efficiently screen for false positives.
7. STPC, or Single Transit Planet Candidate, indicates that the orbital period of the planet is not known and therefore ground-based photometric observations cannot efficiently screen for false positives.
8. NEB, or Nearby Eclipsing Binary, indicates the detection of a NEB that is contaminating the TESS aperture.
9. PNEB indicates a Possible NEB.
10. NPC, or Nearby Planet Candidate, indicates that the TESS detection was actually of a nearby star, but the TESS detection itself is not ruled out to be a false positive. However, the original TOI is retired as a false positive in this case.
11. APC, or Ambiguous Planet Candidate, indicates that results are ambiguous, but suggest that confirming a planet candidate in the system would be difficult.
12. BEB, or Blended Eclipsing Binary, and EB, Eclipsing Binary, indicate the presence of an eclipsing binary as the cause for the TESS detection.
13. FA, or False Alarm, indicates an instrumental anomaly as the cause of the detection.

In this analysis, we consider any TOI with a photometric disposition of PNEB, NEB, NPC, APC, BEB, EB, and FA to be a false positive and remove them from our sample. After this false-positive cut, there are 86 binary systems with exoplanets.

2.2. Visual Binaries from Gaia

2.2.1. Control Sample of Visual Binaries without Planet Candidates

We also identified a control sample of visual binary systems from the El-Badry & Rix (2018) catalog. Kepler has taught us that most of these stars likely host planetary systems of their own (e.g., Fressin et al. 2013; Deacon et al. 2016), but since they do not host any transiting planets, their inclinations will be unknown. Therefore, performing our analysis on a control sample and comparing the results against the sample of binaries with planet candidates helps give us confidence that any features we see in the resulting distribution of inclination angles are astrophysical and not due to selection effects. We specifically constructed our control sample to have nearly identical properties to the sample of binaries with planet candidates to make sure that our control sample incorporates any selection biases from the TESS planet-detection process.

Table 1
Facilities Used for SG1 Seeing-limited Photometric Follow-up Observations

Observatory/Telescope	Location	Aperture (m)	Pixel Scale (arcsec)	FOV (arcmin^2)
Acton Sky Portal (Private Observatory)	Acton, MA, USA	0.36	0.69	17.3 × 11.5
Adams Observatory at Austin College	Sherman, TX, USA	0.61	0.38	26 × 26
Antarctic Search for Transiting ExoPlanets (ASTEP)	Concordia Station, Antarctica	0.4	0.93	63 × 63
Chilean-Hungarian Automated Telescope (CHAT)	Las Campanas Observatory, Chile	0.7	0.6	21 × 21
Deep Sky West	Rowe, NM, USA	0.5	1.09	37 × 37
El Sauce Observatory (Evans Private Telescope)	Coquimbo, Chile	0.36	1.47	19 × 13
Fred L. Whipple Observatory (FLWO)	Amado, Arizona, USA	1.2	0.672	23.1 × 23.1
George Mason University (GMU)	Fairfax, Virginia, USA	0.8	0.35	23 × 23
Grand-Pra Observatory	Valais Sion, Switzerland	0.4	0.73	12.9 × 12.55
Hazelwood Private Observatory	Churchill, Victoria, Australia	0.32	0.55	20 × 14
Infrared Survey Facility (IRSF/SIRIUS)	South Africa	1.4	0.45	7.7 × 7.7
Las Cumbres Observatory Global Telescope (0.4 m)	Spain, Australia	0.4	0.571	29.2 × 19.5
Las Cumbres Observatory Global Telescope (1 m)	Chile, South Africa, Australia, USA	1.0	0.39	26 × 26
Las Cumbres Observatory Global Telescope (2 m/MuSCAT3)	Haleakala, Hawaii, USA	2.0	0.27	9.5 × 9.5
MEarth-South Observatory	La Serena, Chile	0.4	0.84	29 × 29
Mt. Kent Observatory (CDK700)	Toowoomba, Australia	0.7	0.4	27 × 27
Mt. Stuart Observatory	Dunedin, New Zealand	0.3175	0.88	44 × 30
Mt. Lemmon Observatory	Tucson, AZ, USA	0.61	0.39	26 × 26
Observatoire du Mont-Mégantic (OMM)	Notre-Dame-des-Bois, Québec, Canada	1.6	0.47	7.95 × 7.95
Observatori Astronòmic Albanyà (OAA)	Albanyà, Girona, Spain	0.406	1.44	36 × 36
Okayama 188 cm Telescope (MuSCAT)	Okayama, Japan	1.88	0.358	6.1 × 6.1
Perth Exoplanet Survey Telescope (PEST)	Perth, Australia	0.3	1.2	31 × 21
Kotizarovci Observatory	Sarsoni, Croatia	0.3	1.21	15 × 10
Private observatory of the Mount	Saint-Pierre-du-Mont, France	0.20	0.69	38 × 29
Sierra Nevada Observatory	Granada, Andalucía, Spain	1.5	0.232	7.92 × 7.92
Teide Observatory (MuSCAT2)	La Laguna, Spain	1.52	0.44	7.4 × 7.4
TRAPPIST-North	Oukaimeden Observatory, Morocco	0.6	0.64	22 × 22
Virtual Telescope Project	Ceccano, Italy	0.43	1.2	16 × 11
Whitin Observatory at Wellesley College	Wellesley, MA USA	0.7	0.67	23 × 23

To achieve this goal, we defined a metric, $\mathcal{M}$, to quantify the similarity between any two visual binary systems:

$$\mathcal{M} = \left(\frac{\Delta G_1}{4}\right)^2 + \left(\frac{\Delta G_2}{4}\right)^2 + \left(\frac{\Delta RP_1}{4}\right)^2 + \left(\frac{\Delta RP_2}{4}\right)^2 + \left(\frac{\Delta BP_1}{4}\right)^2 + \left(\frac{\Delta BP_2}{4}\right)^2 + (\Delta\varpi)^2 + (\Delta s)^2, \quad (3)$$

where s is the projected separation of the two stars in the binary system, ϖ the system parallax, and G, BP and RP are the stars' apparent magnitudes in the three Gaia passbands. Here, the Δ symbol represents the normalized fractional difference between the values for the two systems: a system with a transiting exoplanet and potential control sample system, and the subscripts 1 and 2 represent the primary and secondary star in each system. For instance, $\Delta G_1 = \frac{(G_1 - G_c)}{G_c}$, where c represents the control sample. We arbitrarily divide all magnitude normalized differences by 4 so that not all weight is given to the magnitudes.

For each of the visual binary systems with non-false-positive exoplanets as of 2020 December 25, we identified the 12 systems from the El-Badry & Rix (2018) catalog with the lowest $\mathcal{M}$ metric. Systems were not removed after each sampling procedure (i.e., they are allowed to be included twice); however, due to the large number of systems present in the El-Badry & Rix (2018) catalog, the resulting control sample has no repeated systems. A subset of our planet-candidate sample was also identified by El-Badry & Rix (2019) to have spectroscopic metallicity measurements from one of several large spectroscopic surveys (see Section 2.3.1). For these systems, we restricted our search for similar systems to those that also have an archival spectroscopic metallicity measurement from El-Badry & Rix (2019). In total, we identify a control sample of 960 systems with very similar distributions of parameters to the input sample of binaries containing planet candidates. Figure 3 shows various properties of the sample with exoplanets and control sample.

2.2.2. Astrometric Parameters

Our analysis hinges on highly precise measurements of the positions, proper motions, and parallaxes of each star in the visual binary system. Originally we used parameters from Gaia Data Release 2 (DR2; Gaia Collaboration et al. 2018; Lindegren et al. 2018), which were based on 22 months of data. During the preparation of our manuscript, updated astrometric parameters based on 34 months of data became available in Gaia EDR3 (Gaia Collaboration et al. 2021; Lindegren et al. 2021). We performed our full analysis using data from both Gaia DR2 and EDR3 and found consistent results between the two samples. We present the results from our analysis using the more precise Gaia EDR3 data in the rest of this paper.

2.2.3. Removing Incorrect Cross-matches, High-RUWE Solutions, and White Dwarfs

We apply a variety of cuts to both the control sample and sample with exoplanets in order to ensure that only high-quality astrometric parameters are preserved.

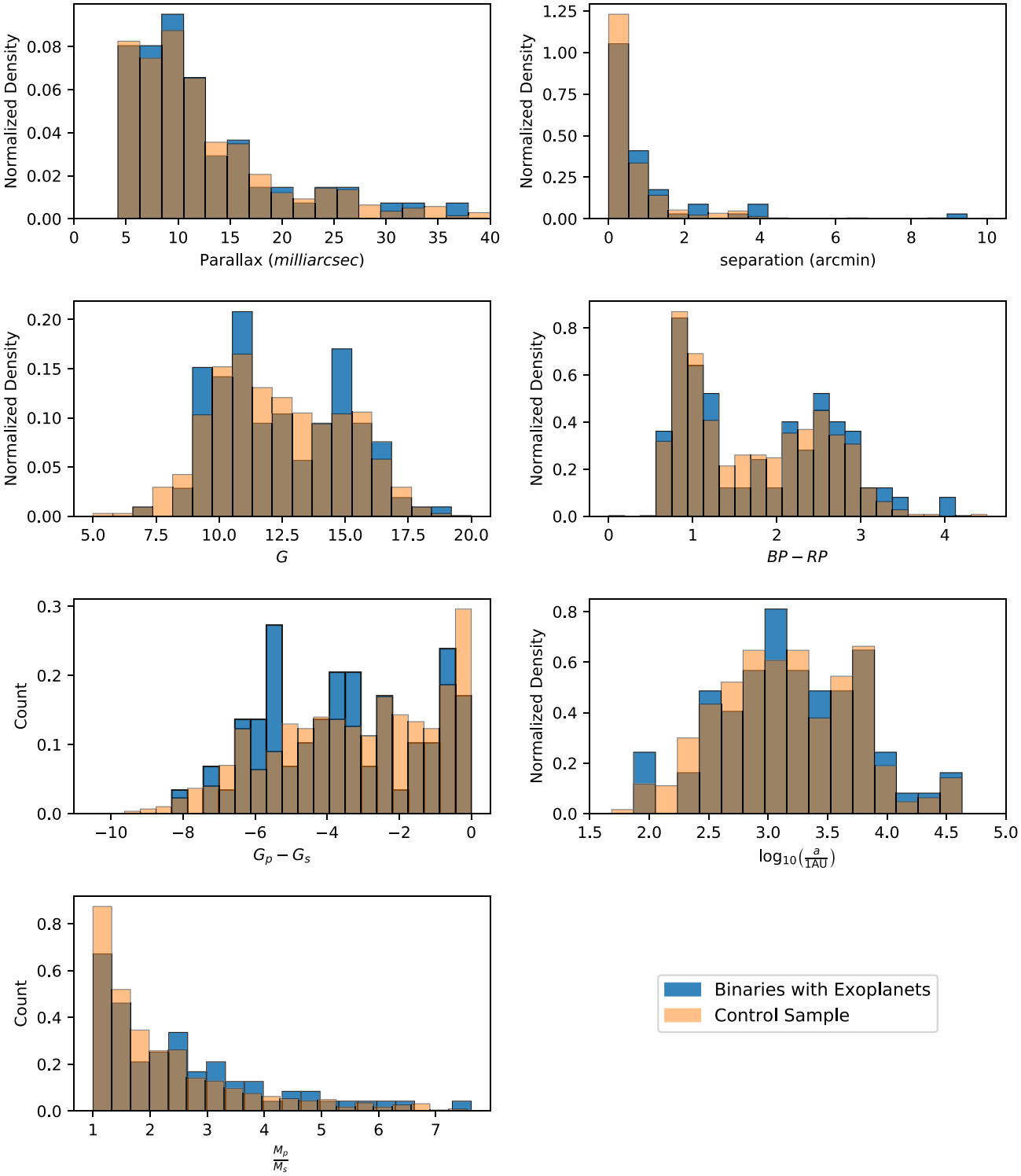

Figure 3. Histograms of properties of the binary systems. From left to right: parallax in milliarcseconds, projected separation in arcminutes, apparent G magnitude, $BP - RP$ color, $G_p - G_s$, where p is the primary star (defined as the brighter star) and s is the secondary star, $\log_{10}(a)$ where a is the projected semimajor axis, and mass ratio of the primary and secondary star.

In the process of converting between Gaia DR2 and Gaia EDR3 IDs, a purely positional cross-match can contaminate the sample due to proper motion movement from the Gaia DR2 epoch (2015.5) to the Gaia EDR3 epoch (2016) and the addition of new sources in EDR3. To ensure that there are no incorrectly cross-matched stars in our sample, we exclude 17 binary systems in the control sample for which $|G_{\mathrm{EDR3}} - G_{\mathrm{DR2}}| > 0.05$.

The renormalized unit weight error (RUWE) can be used as an indicator of the quality of the Gaia astrometric solution for a star (Lindegren 2018). The RUWE is the square root of the

reduced χ^2 divided by a correction function that eliminates dependence on G magnitude and $BP - RP$ color. An RUWE of greater than 1.4 typically indicates a poor astrometric fit, so we eliminate any systems for which the RUWE for at least one of the stars is greater than 1.4. A high RUWE can indicate the presence of an unresolved companion (Belokurov et al. 2020).

We also remove any binaries where either the host star or companion star is a white dwarf; it is more difficult to estimate masses for white dwarfs than for main-sequence stars, and in these systems the binary orbit has been influenced by post-main-sequence mass loss. While these effects are very interesting in their own right, it is beyond the scope of this work to consider them.

After these cuts, there are 67 binary systems with exoplanets and 688 binary systems in the control sample. The distribution of the radii and the periods of the exoplanets in our sample are shown in Figure 4.

2.2.4. Other Work Identifying Visual Binaries in Gaia

The El-Badry & Rix (2018) catalog we used in this study is not the only list of visual binary stars including planet candidates. Recently, Mugrauer & Michel (2020) presented a sample of 193 binary companions of TESS exoplanets. Although Mugrauer & Michel (2020) identify a significantly larger number of possible binary companions to TOIs, they do not identify visual binaries in non-planet-hosting stars with the same criteria that we could use to construct a control sample, so we cannot include these additional binaries in our analysis. Ziegler et al. (2020) used speckle imaging with the Southern Astrophysical Research Observatory to search for binary companions to TOIs. They then compared their discovered companions to those discovered in Gaia DR2. Many of their systems overlap with our sample.

During the final preparation of our manuscript, El-Badry et al. (2021) reported an updated search for visual binaries using the more precise astrometric parameters from Gaia EDR3, including a significant increase in the number of identified systems. In the future, we could perform the same analysis in this paper on their larger sample of visual binaries and potentially increase the statistical significance of our results. We checked and found that most of the binary systems (92%) in our sample lie in the sample of El-Badry et al. (2021), with the inclination distribution being virtually the same when excluding those systems not in El-Badry et al. (2021).

2.3. Ground-based Spectroscopy

Fitting binary orbits using only instantaneous positions and proper motions from Gaia requires an estimate of the mass of each binary component, which in turn requires an estimate of each star's metallicity. To derive the metallicities of stars in our samples, we use both archival observations from large spectroscopic surveys and targeted follow-up observations of planet-candidate host stars made by the TESS Follow-up Observing Program (TFOP). Below, we describe the sources of our spectroscopic parameters and the procedure we used to determine the metallicities of the observed stars. Because the components of relatively wide-binary stars are known to have nearly identical elemental abundances in most cases (Hawkins et al. 2020), we assume the metallicity of both stars in the binary are the same when we only have metallicity measurements for one of the pair.

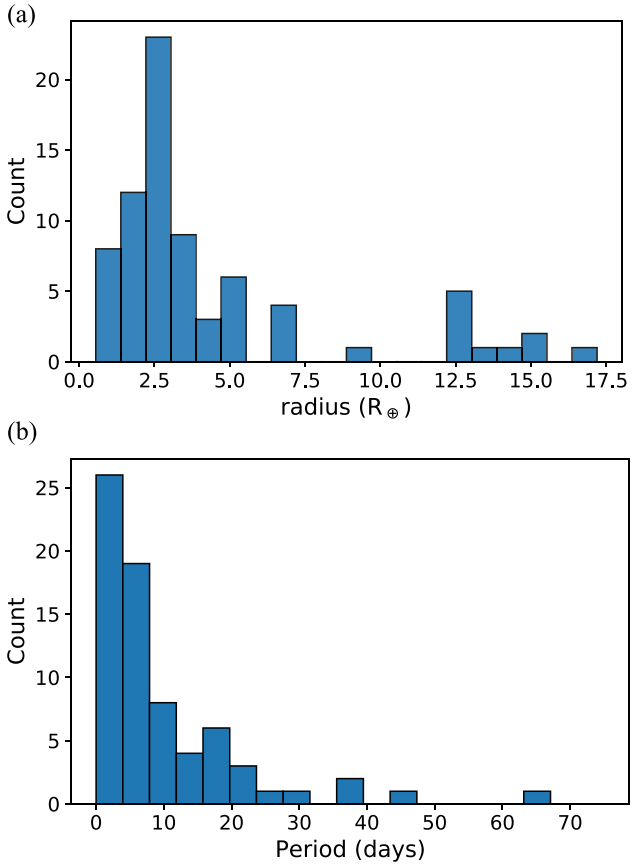

Figure 4. Most of the planets in our sample are small (1–5 $R_\oplus$), and thus have relatively low false-positive probabilities (e.g., Morton & Johnson 2011; Guerrero et al. 2021) compared to giant planet candidates (Santerne et al. 2012).

For stars that have more than one spectroscopic observation, we use an average of the metallicities derived from the separate spectroscopic observations and add the errors from each separate observation in quadrature.

2.3.1. Archival Spectroscopy

Many of the stars in our samples have archival spectra and published metallicity estimates. El-Badry & Rix (2019) cross-matched their sample of visual binary stars (El-Badry & Rix 2018) with stars observed by large spectroscopic surveys and identify a subset of 8507 binaries for which spectroscopic metallicities have been reported in the literature for at least one component. The archival metallicities they identify come from the following surveys or compilations: RAVE (Steinmetz 2003; Kunder et al. 2017), LAMOST (Zhao et al. 2012), Hypatia (Hinkel et al. 2014), APOGEE (Majewski et al. 2016), and GALAH (Buder et al. 2018; Čotar et al. 2019). Of the stars in our sample of binary stars with planet candidates, 16 stars have a metallicity from RAVE, one from LAMOST, four from the Hypatia catalog, two from APOGEE, and two from GALAH.

2.3.2. Las Cumbres Observatory/Network of Robotic Echelle Spectrographs

We obtained observations of seven stars from our sample of binary stars with planet candidates using the Network of Robotic Echelle Spectrographs (NRES), a set of four identical